AJMS
Asian Journal of Mathematical Sciences

RESEARCH ARTICLE

ON OPTIMIZATION OF TECHNOLOGICAL PROCESS TO INCREASE INTEGRATION RATE OF FIELD-EFFECT HETEROTRANSISTORS FRAMEWORK A DOUBLE-TAIL DYNAMIC COMPARATOR

*** E.L. Pankratov**

Nizhny Novgorod State Agrotechnical University, 97 Gagarin avenue, Nizhny Novgorod, 603950, Russia

Corresponding Email: elp2004@mail.ru

Received: 08-10-2025; Revised: 14-11-2025; Accepted: 24-12-2025

ABSTRACT

In this paper we introduce an approach to increase integration rate of field-effect heterotransistors in the framework of a double-tail dynamic comparator. In the framework of the approach we consider a heterostructure with special configuration. Sev-eral specific areas of the heterostructure should be doped by diffusion or ion implantation. Annealing of dopant and/or radiation defects should be optimized.

Keywords: field-effect heterotransistors; On approach to increase integration rate of field-effect heterotransistors in the framework of a double-tail dynamic comparator; optimization of manufacturing; analytical approach for prognosis.

INTRODUCTION

An actual and intensively solving problems of solid state electronics is increasing of integration rate of elements of integrated circuits (p-n-junctions, their systems et al) [1-8]. Increasing of the integration rate leads to necessity to decrease their dimensions. To decrease the dimensions are using several approaches. They are widely using laser and microwave types of annealing of infused dopants. These types of annealing are also widely using for annealing of radiation defects, generated during ion implantation [9-17]. Using the approaches gives a possibility to increase integration rate of elements of integrated circuits through inhomogeneity of technological parameters due to generating inhomogenous distribution of temperature. In this situation one can obtain decreasing dimensions of elements of integrated circuits [18] with account Arrhenius law [1,3]. Another approach to manufacture elements of integrated circuits with smaller dimensions is doping of heterostructure by diffusion or ion implantation [1-3]. However in this case optimization of dopant and/or radiation defects is required [18].

In this paper we consider a heterostructure. The heterostructure consist of a substrate and several epitaxial layers. Some sections have been manufactured in the epitaxial layers. Further we consider doping of these sections by diffusion or ion implantation. The doping gives a possibility to manufacture field-effect

heterotransistors framework a double-tail dynamic comparator so as it is shown on Figs. 1. The manufacturing gives a possibility to increase density of elements of the integrator circuit.

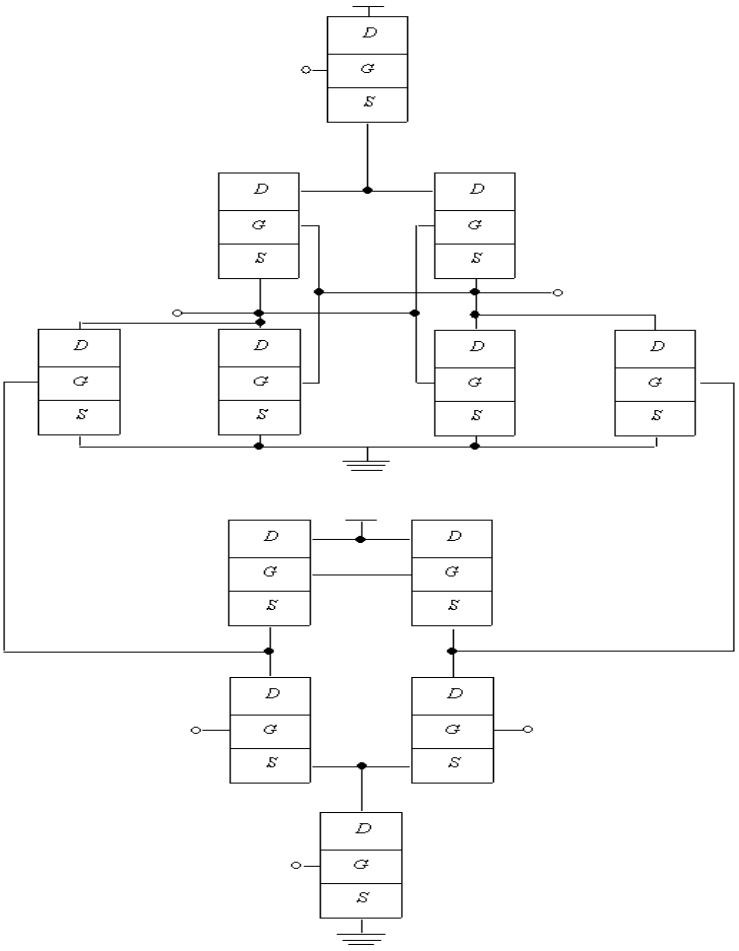

Fig. 1. The considered comporator [15]

After the considered doping dopant and/or radiation defects should be annealed. In the framework of the paper we analyzed dynamics of redistribution of dopant and/or radiation defects during their annealing. We introduce an approach to decrease dimensions of the element. However it is necessary to complicate technological process.

METHODOLOGY

In this section we determine spatio-temporal distributions of concentrations of infused and implanted dopants. To determine these distributions we calculate appropriate solutions of the second Fick's law [1,3,18]

$$\frac{\partial C(x,y,z,t)}{\partial t} =$$

$$= \frac{\partial}{\partial x}\left[D_C \frac{\partial C(x,y,z,t)}{\partial x} \right] + \frac{\partial}{\partial y}\left[D_C \frac{\partial C(x,y,z,t)}{\partial y} \right] + \frac{\partial}{\partial z}\left[D_C \frac{\partial C(x,y,z,t)}{\partial z} \right] \qquad (1)$$

1.1 Boundary and initial conditions for the equations are

$$\left.\frac{\partial C(x,y,z,t)}{\partial x}\right|_{x=0}=0\ \left.\frac{\partial C(x,y,z,t)}{\partial x}\right|_{x=L_x}=0\ \left.\frac{\partial C(x,y,z,t)}{\partial y}\right|_{y=0}=0\ \left.\frac{\partial C(x,y,z,t)}{\partial y}\right|_{x=L_y}=0$$

$$\left.\frac{\partial C(x,y,z,t)}{\partial z}\right|_{z=0}=0\ \left.\frac{\partial C(x,y,z,t)}{\partial z}\right|_{x=L_z}=0\quad C(x,y,z,0)=f(x,y,z). \tag{2}$$

The function C(x,y,z,t) describes the spatio-temporal distribution of concentration of dopant; T is the temperature of annealing; DC is the dopant diffusion coefficient. Value of dopant diffusion coefficient could be changed with changing materials of heterostructure, with changing temperature of materials (including annealing), with changing concentrations of dopant and radiation defects. We approximate dependences of dopant diffusion coefficient on parameters by the following relation with account results in Refs. [20-22]

$$D_C=D_L(x,y,z,T)\left[1+\xi\frac{C^{\gamma}(x,y,z,t)}{P^{\gamma}(x,y,z,T)}\right]\left[1+\varsigma_1\frac{V(x,y,z,t)}{V^*}+\varsigma_2\frac{V^2(x,y,z,t)}{(V^*)^2}\right] \tag{3}$$

Here the function DL (x,y,z,T) describes the spatial (in heterostructure) and temperature (due to Arrhenius law) dependences of diffusion coefficient of dopant. The function P (x,y,z,T) describes the limit of solubility of dopant. Parameter $\gamma\in[1,3]$ describes average quantity of charged defects interacted with atom of dopant [20]. The function V (x,y,z,t) describes the spatio-temporal distribution of concentration of radiation vacancies. Parameter V* describes the equilibrium distribution of concentration of vacancies. The considered concentrational dependence of dopant diffusion coefficient has been described in details in [20]. It should be noted, that using diffusion type of doping did not generation radiation defects. In this situation $\zeta1=\zeta2=0$. We determine spatio-temporal distributions of concentrations of radiation defects by solving the following system of equations [21,22]

$$\frac{\partial I(x,y,z,t)}{\partial t}=\frac{\partial}{\partial x}\left[D_I(x,y,z,T)\frac{\partial I(x,y,z,t)}{\partial x}\right]+\frac{\partial}{\partial y}\left[D_I(x,y,z,T)\frac{\partial I(x,y,z,t)}{\partial y}\right]+$$

$$+\frac{\partial}{\partial z}\left[D_I(x,y,z,T)\frac{\partial I(x,y,z,t)}{\partial z}\right]-k_{I,V}(x,y,z,T)\,I(x,y,z,t)\,V(x,y,z,t)-$$

$$-k_{I,I}(x,y,z,T)I^2(x,y,z,t) \tag{4}$$

$$\frac{\partial V(x,y,z,t)}{\partial t}=\frac{\partial}{\partial x}\left[D_V(x,y,z,T)\frac{\partial V(x,y,z,t)}{\partial x}\right]+\frac{\partial}{\partial y}\left[D_V(x,y,z,T)\frac{\partial V(x,y,z,t)}{\partial y}\right]+$$

$$+\frac{\partial}{\partial z}\left[D_V(x,y,z,T)\frac{\partial V(x,y,z,t)}{\partial z}\right]-k_{I,V}(x,y,z,T)I(x,y,z,t)\,V(x,y,z,t)+$$

$$+k_{V,V}(x,y,z,T)V^2(x,y,z,t).$$

1.2.Boundary and initial conditions for these equations are

$$\left.\frac{\partial \rho(x,y,z,t)}{\partial x}\right|_{x=0}=0 \quad \left.\frac{\partial \rho(x,y,z,t)}{\partial x}\right|_{x=L_x}=0 \quad \left.\frac{\partial \rho(x,y,z,t)}{\partial y}\right|_{y=0}=0 \quad \left.\frac{\partial \rho(x,y,z,t)}{\partial y}\right|_{y=L_y}=0$$

$$\left.\frac{\partial \rho(x,y,z,t)}{\partial z}\right|_{z=0}=0 \quad \left.\frac{\partial \rho(x,y,z,t)}{\partial z}\right|_{z=L_z}=0 \quad \rho(x,y,z,0)=f_\rho(x,y,z). \tag{5}$$

Here ρ =I,V. The function I (x,y,z,t) describes the spatio-temporal distribution of concentration of radiation interstitials; Dρ(x,y,z,T) are the diffusion coefficients of point radiation defects; terms V2(x,y,z,t) and I2(x,y,z,t) correspond to generation divacancies and diinterstitials; kI,V(x,y,z,T) is the parameter of recombination of point radiation defects; kI,I(x,y,z,T) and kV,V(x,y,z,T) are the parameters of generation of simplest complexes of point radiation defects.

Further we determine distributions in space and time of concentrations of divacancies ΦV(x,y,z,t) and diinterstitials ΦI(x,y,z,t) by solving the following system of equations [21,22]

$$\frac{\partial \Phi_I(x,y,z,t)}{\partial t}=\frac{\partial}{\partial x}\left[D_{\Phi I}(x,y,z,T)\frac{\partial \Phi_I(x,y,z,t)}{\partial x}\right]+\frac{\partial}{\partial y}\left[D_{\Phi I}(x,y,z,T)\frac{\partial \Phi_I(x,y,z,t)}{\partial y}\right]+$$

$$+\frac{\partial}{\partial z}\left[D_{\Phi I}(x,y,z,T)\frac{\partial \Phi_I(x,y,z,t)}{\partial z}\right]+k_{I,I}(x,y,z,T)I^2(x,y,z,t)-k_I(x,y,z,T)I(x,y,z,t) \tag{6}$$

$$\frac{\partial \Phi_V(x,y,z,t)}{\partial t}=\frac{\partial}{\partial x}\left[D_{\Phi V}(x,y,z,T)\frac{\partial \Phi_V(x,y,z,t)}{\partial x}\right]+\frac{\partial}{\partial y}\left[D_{\Phi V}(x,y,z,T)\frac{\partial \Phi_V(x,y,z,t)}{\partial y}\right]+$$

$$+\frac{\partial}{\partial z}\left[D_{\Phi V}(x,y,z,T)\frac{\partial \Phi_V(x,y,z,t)}{\partial z}\right]+k_{V,V}(x,y,z,T)V^2(x,y,z,t)-k_V(x,y,z,T)V(x,y,z,t)$$

Boundary and initial conditions for these equations are

$$\left.\frac{\partial \Phi_\rho(x,y,z,t)}{\partial x}\right|_{x=0}=0 \quad \left.\frac{\partial \Phi_\rho(x,y,z,t)}{\partial x}\right|_{x=L_x}=0 \quad \left.\frac{\partial \Phi_\rho(x,y,z,t)}{\partial y}\right|_{y=0}=0 \quad \left.\frac{\partial \Phi_\rho(x,y,z,t)}{\partial y}\right|_{y=L_y}=0$$

$$\left.\frac{\partial \Phi_\rho(x,y,z,t)}{\partial z}\right|_{z=0}=0 \quad \left.\frac{\partial \Phi_\rho(x,y,z,t)}{\partial z}\right|_{z=L_z}=0$$

$$\Phi_I(x,y,z,0)=f_{\Phi I}(x,y,z),\ \Phi_V(x,y,z,0)=f_{\Phi V}(x,y,z). \tag{7}$$

Here DΦρ(x,y,z,T) are the diffusion coefficients of the above complexes of radiation defects; kI(x,y,z,T) and kV(x,y,z,T) are the parameters of decay of these complexes.

We calculate distributions of concentrations of point radiation defects in space and time by recently elaborated approach [18]. The approach based on transformation of approximations of diffusion coefficients in the following form: Dρ(x,y,z,T)=D0ρ[1+ερ gρ(x,y,z,T)], where D0ρ are the average values of diffusion coefficients, 0≤ερ<1, |gρ(x, y,z,T)|≤1, ρ =I,V. We also used analogous transformation of

approximations of parameters of recombination of point defects and parameters of generation of their complexes: kI,V(x,y,z,T)=k0I,V[1+εI,V gI,V(x,y,z,T)], kI,I(x,y,z,T)=k0I,I [1+εI,I gI,I(x,y,z,T)] and kV,V(x,y,z,T)=k0V,V [1+εV,V gV,V(x,y,z,T)], where k0ρ1,ρ2 are the their average values, 0≤εI,V <1, 0≤εI,I <1, 0≤εV,V<1, | gI,V(x,y,z,T)|≤1, | gI,I(x,y,z,T)|≤1, |gV,V(x,y,z,T)|≤1. Let us introduce the following dimensionless variables: $\widetilde{I}\left(x,y,z,t\right)=I\left(x,y,z,t\right)/I^{*}$, $\widetilde{V}\left(x,y,z,t\right)=\ =V\left(x,y,z,t\right)/V^{*}$, $\omega=L^{2}k_{0I,V}\left/\sqrt{D_{0I}D_{0V}}\right.$, $\Omega_{\rho}=L^{2}k_{0\rho,\rho}\left/\sqrt{D_{0I}D_{0V}}\right.$, $\vartheta=\sqrt{D_{0I}D_{0V}}\,t/L^{2}$, χ = x/Lx, η = y /Ly, ϕ = z/Lz. The introduction leads to transformation of Eqs.(4) and conditions (5) to the following form

$$\frac{\partial\widetilde{I}\left(\chi,\eta,\phi,\vartheta\right)}{\partial\vartheta}=\frac{D_{0I}}{\sqrt{D_{0I}D_{0V}}}\frac{\partial}{\partial\chi}\left\{\left[1+\varepsilon_{I}g_{I}\left(\chi,\eta,\phi,T\right)\right]\frac{\partial\widetilde{I}\left(\chi,\eta,\phi,\vartheta\right)}{\partial\chi}\right\}+\frac{\partial}{\partial\eta}\left\{\left[1+\varepsilon_{I}g_{I}\left(\chi,\eta,\phi,T\right)\right]\times\right.$$

$$\left.\times\frac{\partial\widetilde{I}\left(\chi,\eta,\phi,\vartheta\right)}{\partial\eta}\right\}\frac{D_{0I}}{\sqrt{D_{0I}D_{0V}}}+\frac{D_{0I}}{\sqrt{D_{0I}D_{0V}}}\frac{\partial}{\partial\phi}\left\{\left[1+\varepsilon_{I}g_{I}\left(\chi,\eta,\phi,T\right)\right]\frac{\partial\widetilde{I}\left(\chi,\eta,\phi,\vartheta\right)}{\partial\phi}\right\}-\widetilde{I}\left(\chi,\eta,\phi,\vartheta\right)\times$$

$$\times\omega\left[1+\varepsilon_{I,V}g_{I,V}\left(\chi,\eta,\phi,T\right)\right]\widetilde{V}\left(\chi,\eta,\phi,\vartheta\right)-\Omega_{I}\left[1+\varepsilon_{I,I}g_{I,I}\left(\chi,\eta,\phi,T\right)\right]\widetilde{I}^{2}\left(\chi,\eta,\phi,\vartheta\right) \tag{8}$$

$$\frac{\partial\widetilde{V}\left(\chi,\eta,\phi,\vartheta\right)}{\partial\vartheta}=\frac{D_{0V}}{\sqrt{D_{0I}D_{0V}}}\frac{\partial}{\partial\chi}\left\{\left[1+\varepsilon_{V}g_{V}\left(\chi,\eta,\phi,T\right)\right]\frac{\partial\widetilde{V}\left(\chi,\eta,\phi,\vartheta\right)}{\partial\chi}\right\}+\frac{\partial}{\partial\eta}\left\{\left[1+\varepsilon_{V}g_{V}\left(\chi,\eta,\phi,T\right)\right]\times\right.$$

$$\left.\times\frac{\partial\widetilde{V}\left(\chi,\eta,\phi,\vartheta\right)}{\partial\eta}\right\}\frac{D_{0V}}{\sqrt{D_{0I}D_{0V}}}+\frac{D_{0V}}{\sqrt{D_{0I}D_{0V}}}\frac{\partial}{\partial\phi}\left\{\left[1+\varepsilon_{V}g_{V}\left(\chi,\eta,\phi,T\right)\right]\frac{\partial\widetilde{V}\left(\chi,\eta,\phi,\vartheta\right)}{\partial\phi}\right\}-\widetilde{I}\left(\chi,\eta,\phi,\vartheta\right)\times$$

$$\times\omega\left[1+\varepsilon_{I,V}g_{I,V}\left(\chi,\eta,\phi,T\right)\right]\widetilde{V}\left(\chi,\eta,\phi,\vartheta\right)-\Omega_{V}\left[1+\varepsilon_{V,V}g_{V,V}\left(\chi,\eta,\phi,T\right)\right]\widetilde{V}^{2}\left(\chi,\eta,\phi,\vartheta\right)$$

$$\left.\frac{\partial\widetilde{\rho}\left(\chi,\eta,\phi,\vartheta\right)}{\partial\chi}\right|_{\chi=0}=0\ \left.\frac{\partial\widetilde{\rho}\left(\chi,\eta,\phi,\vartheta\right)}{\partial\chi}\right|_{\chi=1}=0\ \left.\frac{\partial\widetilde{\rho}\left(\chi,\eta,\phi,\vartheta\right)}{\partial\eta}\right|_{\eta=0}=0\ \left.\frac{\partial\widetilde{\rho}\left(\chi,\eta,\phi,\vartheta\right)}{\partial\eta}\right|_{\eta=1}=0$$

$$\left.\frac{\partial\widetilde{\rho}\left(\chi,\eta,\phi,\vartheta\right)}{\partial\phi}\right|_{\phi=0}=0\ \left.\frac{\partial\widetilde{\rho}\left(\chi,\eta,\phi,\vartheta\right)}{\partial\phi}\right|_{\phi=1}=0\ \widetilde{\rho}\left(\chi,\eta,\phi,\vartheta\right)=\frac{f_{\rho}\left(\chi,\eta,\phi,\vartheta\right)}{\rho^{*}} \tag{9}$$

We determine solutions of Eqs.(8) with conditions (9) framework recently introduced approach [18], i.e. as the power series

$$\widetilde{\rho}\left(\chi,\eta,\phi,\vartheta\right)=\sum_{i=0}^{\infty}\varepsilon_{\rho}^{i}\sum_{j=0}^{\infty}\omega^{j}\sum_{k=0}^{\infty}\Omega_{\rho}^{k}\widetilde{\rho}_{ijk}\left(\chi,\eta,\phi,\vartheta\right). \tag{10}$$

Substitution of the series (10) into Eqs.(8) and conditions (9) gives us possibility to obtain equations for initial-order approximations of concentration of point defects $\widetilde{I}_{000}\left(\chi,\eta,\phi,\vartheta\right)$ and $\widetilde{V}_{000}\left(\chi,\eta,\phi,\vartheta\right)$ and corrections for them $\widetilde{I}_{ijk}\left(\chi,\eta,\phi,\vartheta\right)$ and $\widetilde{V}_{ijk}\left(\chi,\eta,\phi,\vartheta\right)$, i ≥1, j ≥1, k ≥1. The equations are presented in the

Appendix. Solutions of the equations could be obtained by standard Fourier approach [24,25]. The solutions are presented in the Appendix.

Now we calculate distributions of concentrations of simplest complexes of point radiation defects in space and time. To determine the distributions we transform approximations of diffusion coefficients in the following form: $D\Phi\rho(x,y,z,T)=D0\Phi\rho[1+ \varepsilon\Phi\rho g\Phi\rho(x,y,z,T)]$, where $D0\Phi\rho$ are the average values of diffusion coefficients. In this situation the Eqs.(6) could be written as

$$\frac{\partial \Phi_I(x,y,z,t)}{\partial t} = D_{0\Phi I}\frac{\partial}{\partial x}\left\{\left[1+\varepsilon_{\Phi I} g_{\Phi I}(x,y,z,T)\right]\frac{\partial \Phi_I(x,y,z,t)}{\partial x}\right\} + k_{I,I}(x,y,z,T)\, I^2(x,y,z,t) +$$

$$+ D_{0\Phi I}\frac{\partial}{\partial y}\left\{\left[1+\varepsilon_{\Phi I} g_{\Phi I}(x,y,z,T)\right]\frac{\partial \Phi_I(x,y,z,t)}{\partial y}\right\} + D_{0\Phi I}\frac{\partial}{\partial z}\left\{\left[1+\varepsilon_{\Phi I} g_{\Phi I}(x,y,z,T)\right]\frac{\partial \Phi_I(x,y,z,t)}{\partial z}\right\} -$$

$$- k_I(x,y,z,T) I(x,y,z,t)$$

$$\frac{\partial \Phi_V(x,y,z,t)}{\partial t} = D_{0\Phi V}\frac{\partial}{\partial x}\left\{\left[1+\varepsilon_{\Phi V} g_{\Phi V}(x,y,z,T)\right]\frac{\partial \Phi_V(x,y,z,t)}{\partial x}\right\} + k_{I,I}(x,y,z,T)\, I^2(x,y,z,t) +$$

$$+ D_{0\Phi V}\frac{\partial}{\partial y}\left\{\left[1+\varepsilon_{\Phi V} g_{\Phi V}(x,y,z,T)\right]\frac{\partial \Phi_V(x,y,z,t)}{\partial y}\right\} + D_{0\Phi V}\frac{\partial}{\partial z}\left\{\left[1+\varepsilon_{\Phi V} g_{\Phi V}(x,y,z,T)\right]\frac{\partial \Phi_V(x,y,z,t)}{\partial z}\right\} -$$

$$- k_I(x,y,z,T)\, I(x,y,z,t)$$

Farther we determine solutions of above equations as the following power series

$$\Phi_\rho(x,y,z,t) = \sum_{i=0}^{\infty} \varepsilon_{\Phi\rho}^i \Phi_{\rho i}(x,y,z,t). \tag{11}$$

Now we used the series (11) into Eqs.(6) and appropriate boundary and initial conditions. The using gives the possibility to obtain equations for initial-order approximations of concentrations of complexes of defects $\Phi\rho0(x,y,z,t)$, corrections for them $\Phi\rho i(x,y,z,t)$ (for them $i \geq 1$) and boundary and initial conditions for them. We remove equations and conditions to the Appendix. Solutions of the equations have been calculated by standard approaches [24,25] and presented in the Appendix.

Now we calculate distribution of concentration of dopant in space and time by using the approach, which was used for analysis of radiation defects. To use the approach we consider following transformation of approximation of dopant diffusion coefficient: $DL(x,y,z,T)=D0L[1+ \varepsilon LgL(x,y,z,T)]$, where $D0L$ is the average value of dopant diffusion coefficient, $0 \leq \varepsilon L < 1$, $|gL(x,y,z,T)| \leq 1$. Farther we consider solution of Eq.(1) as the following series:

$$C(x,y,z,t) = \sum_{i=0}^{\infty} \varepsilon_L^i \sum_{j=1}^{\infty} \xi^j C_{ij}(x,y,z,t).$$

Using the relation into Eq.(1) and conditions (2) leads to obtaining equations for the functions $Cij(x,y,z,t)$ ($i \geq 1$, $j \geq 1$), boundary and initial conditions for them. The equations are presented in the Appendix. Solutions of the equations have been calculated by standard approaches (see, for example, [24,25]). The

solutions are presented in the Appendix.

We analyzed distributions of concentrations of dopant and radiation defects in space and time analytically by using the second-order approximations on all parameters, which have been used in appropriate series. Usually the second-order approximations are enough good approximations to make qualitative analysis and to obtain quantitative results. All analytical results have been checked by numerical simulation.

DISCUSSION OF RESULTS

In this section we analyzed spatio-temporal distributions of concentrations of dopants.

Figs. 2 shows typical spatial distributions of concentrations of dopants in neighborhood of interfaces of heterostructures. We calculate these distributions of concentrations of dopants under the following condition: value of dopant diffusion coefficient in doped area is larger, than value of dopant diffusion coefficient in nearest areas. In this situation one can find increasing of compactness of field-effect transistors with increasing of homogeneity of distribution of concentration of dopant at one time. Changing relation between values of dopant diffusion coefficients leads to opposite result (see Figs. 3).

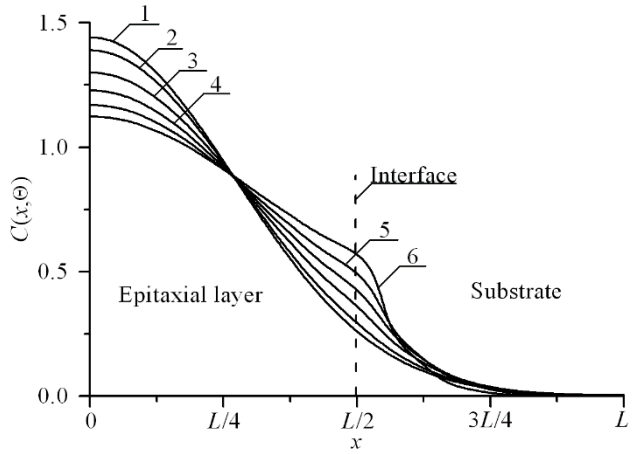

Fig. 2a. Dependences of concentration of dopant, infused in heterostructure from Figs. 1, on coordinate in direction, which is perpendicular to interface between epitaxial layer substrate. Difference between values of dopant diffusion coefficient in layers of heterostructure increases with increasing of number of curves. Value of dopant diffusion coefficient in the epitaxial layer is larger, than value of dopant diffusion coefficient in the substrate

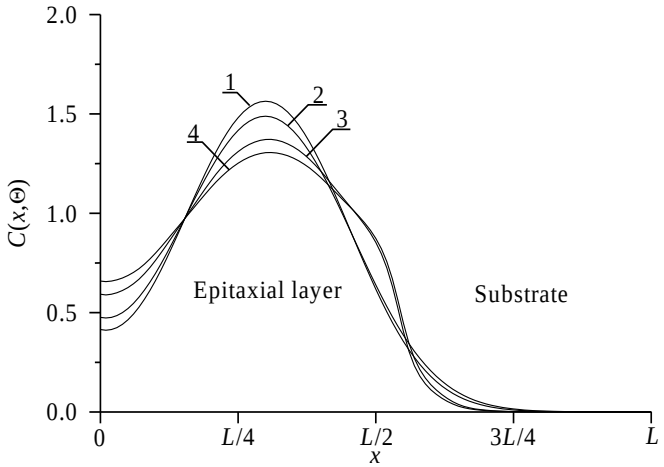

Fig. 2b. Dependences of concentration of dopant, implanted in heterostructure from Figs. 1, on coordinate in direction, which is perpendicular to interface between epitaxial layer substrate. Difference between values of dopant diffusion coefficient in layers of heterostructure increases with increasing of number of curves. Value of dopant diffusion coefficient in the epitaxial layer is larger, than value of dopant diffusion coefficient in the substrate. Curve 1 corresponds to homogenous sample and annealing time Θ = 0.0048 (Lx2+Ly2+Lz2)/D0. Curve 2 corresponds to homogenous sample and annealing time Θ = 0.0057 (Lx2+Ly2+Lz2)/D0. Curves 3 and 4 correspond to heterostructure from Figs. 1; annealing times Θ = 0.0048 (Lx2+Ly2+Lz2)/D0 and Θ = 0.0057 (Lx2 +Ly2+Lz2)/D0, respectively

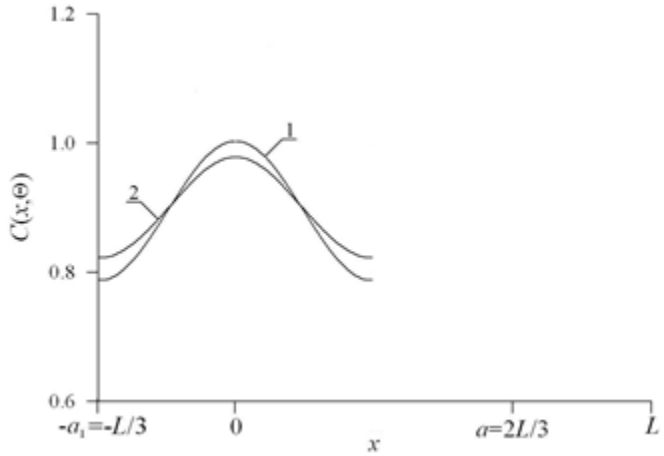

Fig. 3a. Distributions of concentration of dopant, infused in average section of epitaxial layer of heterostructure from Figs. 1 in direction parallel to interface between epitaxial layer and substrate of heterostructure. Difference between values of dopant diffusion coefficients increases with increasing of number of curves. Value of dopant diffusion coefficient in this section is smaller, than value of dopant diffusion coefficient in nearest sections

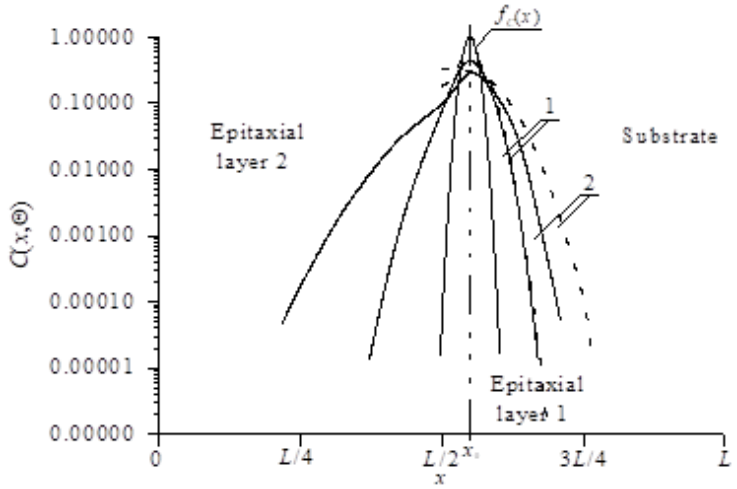

Fig. 3b. Calculated distributions of implanted dopant in epitaxial layers of heterostructure. Solid lines are spatial distributions of implanted dopant in system of two epitaxial layers. Dushed lines are spatial distributions of implanted dopant in one epitaxial layer. Annealing time increases with increasing of number of curves

It should be noted, that framework the considered approach one shall optimize annealing of dopant and/or radiation defects. To do the optimization we used recently introduced criterion [26-34]. The optimization based on approximation real distribution by step-wise function ψ (x,y,z) (see Figs. 4). Farther the required values of optimal annealing time have been calculated by minimization the following mean- squared error

$$U = \frac{1}{L_x L_y L_z} \int_0^{L_x} \int_0^{L_y} \int_0^{L_z} \left[C(x,y,z,\Theta) - \psi(x,y,z) \right] d\,z\,d\,y\,d\,x\,. \qquad (12)$$

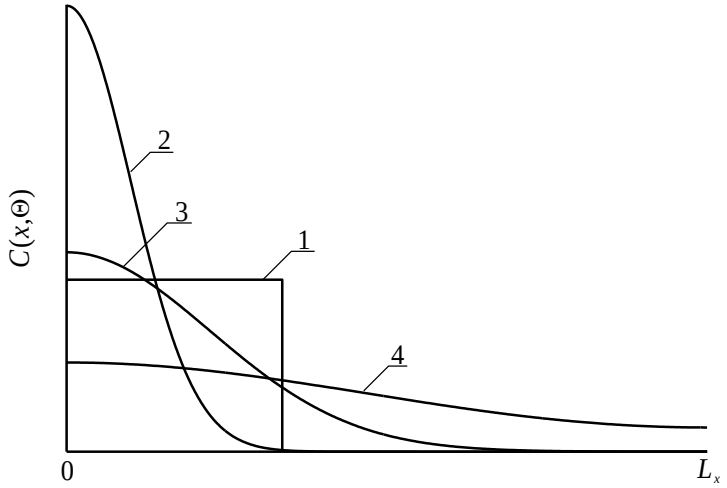

Fig.4a. Distributions of concentration of infused dopant in depth of heterostructure from Fig. 1 for different values of annealing time (curves 2-4) and idealized step-wise approximation (curve 1). Increasing of number of curve corresponds to increasing of annealing time

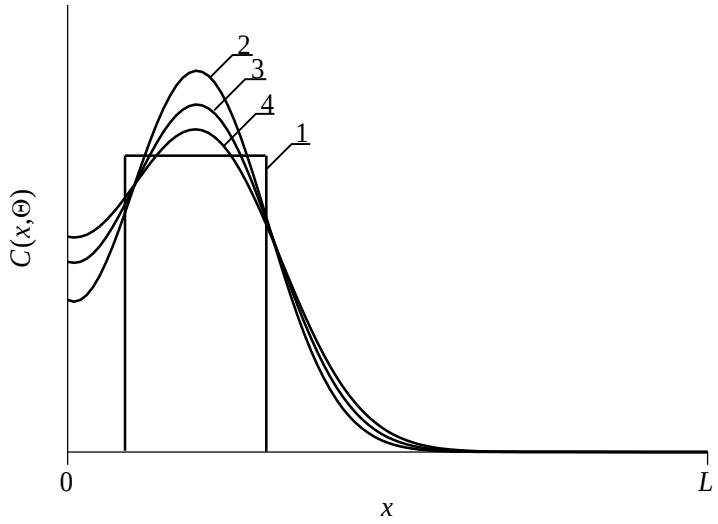

Fig.4b. Distributions of concentration of implanted dopant in depth of hetero-structure from Fig. 1 for different values of annealing time (curves 2-4) and ideal-ized step-wise approximation (curve 1). Increasing of number of curve corre-sponds to increasing of annealing time

We show optimal values of annealing time as functions of parameters on Figs. 5. It is known, that standard step of manufactured ion-doped structures is an-nealing of radiation defects. In the ideal case after finishing the annealing dopant achieves interface between layers of heterostructure. If the dopant has no enough time to achieve the interface, it is practicably to anneal the dopant additionally. The Fig. 5b shows the described dependences of optimal values of additional an-nealing time for the same parameters as for Fig. 5a. Necessity to anneal radiation defects leads to smaller values of optimal annealing of implanted dopant in com-parison with optimal annealing time of infused dopant.

METHODOLOGY

The solution to optimal control problems involves the derivation of the optimal control characterization and the use of the forward and backward sweep for the state and control trajectories respectively[9]. By the Pontryagin's maximum, the optimal control can be analytically derived by the optimality condition while the state and control variables can be derived numerically using the Runge-Kutta of order six subject to the adjoint and transversality conditions[10].

1.1: Statement of problem

We considered the generalized Optimal Control problem given below;

$$\max(\min) J(u) = \int_{t_0}^{T} F(t, x_1(t), x_2(t), \ldots, x_n(t), u(t))\, dt \quad (1)$$

subject to : $\dot{x}_1 = g_1(t,x_1(t),x_2(t),...,x_n(t),u(t))$ (2)

$\dot{x}_2 = g_2(t,x_1(t),x_2(t),...,x_n(t),u(t))$ (3)

...

$x_n = g_n(t,x_1(t),x_2(t),...,x_n(t),u(t))$ (4)

$u_{\min} \leq u \leq u_{\max}$ (5)

where $(x_1(t_0),x_2(t_0),...,x_n(t_0)) = (0,0,...,0)^T \in \mathbf{R}^n$.

The Hamiltonian of the constrained optimal control problem is written as

$$H = F(t, x_1(t), x_2(t), \ldots, x_n(t), u(t)) + \sum_{i=1}^{n} \lambda_i g_i(t, x_1(t), x_2(t), \ldots, x_n(t), u(t)), \quad (6)$$

and the optimality, adjoint and transversality conditions are expressed below respectively as

(Optimality) $$\frac{\partial H}{\partial u} = \frac{\partial F}{\partial u} + \sum_{i=1}^{n} \lambda_i \frac{\partial g_i}{\partial u} \quad (7)$$

(Adjoint) (8)

(Transversality), $$\dot{\lambda}_i = -\frac{\partial H}{\partial x_i} = -\frac{\partial F}{\partial x_i} - \sum_{i=1}^{n} \lambda_i \frac{\partial g_i}{\partial x_i}, \quad (9)$$

$\lambda_i(T) = 0, \forall i = 1, 2, \ldots, n$

1.2: 6th Order Runge-Kutta Scheme

The 7-stage Runge-Kutta of order 6 (RK6) iterative scheme was considered for the development of the forward-backward sweep Algorithm for the solution of Optimal control problems[11]. The RK6 enhances the level of accuracy of the results of the optimal control problem with the developed algorithm[12].

$$K_1 = hf(t_k, x_k),$$
$$K_2 = hf\left(t_k + \frac{h}{4}, x_k + \frac{K_1}{4}\right),$$
$$K_3 = hf\left(t_k + \frac{h}{4}, x_k + \frac{K_1 + K_2}{8}\right),$$
$$K_4 = hf\left(t_k + \frac{h}{2}, x_k + \frac{-5K_2 + 8K_3}{6}\right),$$
$$K_5 = hf\left(t_k + \frac{3h}{4}, x_k + \frac{K_1 + K_2 + 4K_4}{8}\right),$$
$$K_6 = hf\left(t_k + \frac{3h}{4}, x_k + \frac{3K_2 + 2K_3 - K_4 + 2K_5}{8}\right),$$
$$K_7 = h\,f\left(t_k + h, x_k + \frac{K_1 - 2K_2 + 4K_3 + 4K_6}{7}\right)$$
$$x_{k+1} = x_k + \frac{7K_1 + 32K_3 + 12K_4 + 16K_5 + 16K_6 + 7K_7}{90}$$

1.3: Forward-Backward Sweep Method

The derivation of the forward-backward sweep requires the discretization of state, control, and adjoint variables along the knots $t_0 \le t_1 \le t_2 \le \cdots \le t_N$, such that $x_i^k = x_i(t_0 + kh)$, $u_s^k = u_s(t_0 + kh)$, and $\lambda_{ji} = \lambda_i(t_0 - jh)$ for $t_k = t_0 + kh$ and $h = (T - t_0)/N$ is the Step-length with N number of grid-points.Therefore, for any argument x_i in the state vector $(x_i^k, x_2^k, \cdots, x_n^k) \in \mathbb{R}^n$ and a unit adjoint variable u_s for $s \in \{1,2,\cdots,m\}$ and the forward sweep of the state variable using the RK6 method is written as:

$$K_{i1} = hg_1(t_k, x_i^k, u_s(k)), \tag{10}$$
$$K_{i2} = hg_2(t_k + \frac{h}{4}, x_i^k + \frac{K_1}{4}, u_s(t_k + \frac{h}{4})), \tag{11}$$
$$K_{i3} = hg_3(t_k + \frac{h}{4}, x_i^k + \frac{1}{8}(K_1 + K_2),\ u_s(t_k + \frac{h}{4})), \tag{12}$$
$$K_{i4} = hg_4(t_k + \frac{h}{2}, x_i^k + \frac{1}{6}(-5K_2 + 8K_3), u_s(t_k + \frac{h}{2})), \tag{13}$$
$$K_{i5} = hg_5(t_k + \frac{3h}{4}, x_i^k + \frac{1}{8}(K_1 + K_2 + 4K_3), u_s(t_k + \frac{3h}{4})), \tag{14}$$
$$K_{i6} = hg_6(t_k + \frac{3h}{4}, x_i^k + \frac{1}{8}(3K_2 + 2K_3 - K_4 + 2K_5), u_s(t_k + \frac{3h}{4})) \tag{15}$$
$$K_{i7} = h\,g_7\left(t_k + h, x_i^k + \frac{1}{7}(K_1 - 2K_2 + 4K_3 + 4K_6),\ u_s(t_k + h)\right) \tag{16}$$
$$x_i^{k+1} = x_i^k + \frac{7K_1 + 32K_3 + 12K_4 + 16K_5 + 16K_6 + 7K_7}{90}. \tag{17}$$

for the subscript of each argument $i = 1,2,\cdots,n$, $r = 1,2,\cdots,m$, the counter $k = 1,2,\cdots,N$. and the functions g_l, $l = 1, 2\cdots7$ are once continuously differentiable within the time interval $[t_0, T]$ $\left(\text{i.e } \frac{\partial g_l}{\partial x_i} \in C^1[t_0, T]\right)$ and K_{il} denoting the dynamical function of the i−th component (argument) and the l−th stage. For the control characterization, the optimal variable is derived using the optimality condition $\frac{\partial H}{\partial u_r} = 0$ such that

$$u_r^* = \min\{\max\{u_{min}, u_r, \}, u_{max}\} \tag{18}$$

The interpolating polynomial or spline [8] of the control variable $u_s(.)$ can be computed as the formula;

$$u(t + \frac{ah}{b}) = \frac{au(t + h) + (b - a)u(t)}{b} \tag{19}$$

The control variable for the forward(+) and backward (-) sweep are approximated respectively as follows;

$$u(t+\frac{ah}{b}) \approx \begin{cases} \frac{u(t+h)+3u(t)}{4} & a=1,b=4 \\ \frac{u(t+h)+u(t)}{2} & a=1,b=2 \\ \frac{3u(t+h)+u(t)}{4} & a=3,b=4 \end{cases} \quad (20)$$

The backward sweep of the adjoint variables using the proposed RK6 method requires the discretization of the adjoint such that for any argument $\lambda_l^j \in (\lambda_1^j, \lambda_2^j, \cdots, \lambda_n^j) \in \mathbb{R}^n$ with a specific control variable u_s attached to each state equation is expressed thus:

$$\dot{\lambda}_i = -\frac{\partial H}{\partial x_i}(t, \lambda_i, x_i, u_s), \quad i = 1, 2, \ldots, n. \quad (21)$$

Deploying the 7-stage RK6 numerical scheme in the discretization of the backward sweep for the adjoint variables yields the following:

$$K_{i1} = -\frac{\partial H}{\partial x_i}(t_j, \lambda_i^j, x_i, u_s(j)), \quad (22)$$

$$K_{i2} = -\frac{\partial H}{\partial x_i}(t_j + \frac{h}{4}, \lambda_i^j + \frac{K_1}{4}, x_i^j + \frac{K_1}{4}, u_s(t_j + \frac{h}{4})), \quad (23)$$

$$K_{i3} = -\frac{\partial H}{\partial x_i}(t_j + \frac{h}{4}, \lambda_i^j + \frac{1}{8}(K_1 + K_2), x_i^j + \frac{1}{8}(K_1 + K_2), u_s(t_j + \frac{h}{4})), \quad (24)$$

$$K_{i4} = -\frac{\partial H}{\partial x_i}(t_j + \frac{h}{2}, \lambda_i^j + \frac{1}{6}(-5K_2 + 8K_3), x_i^j + \frac{1}{6}(-5K_2 + 8K_3), u_s(t_j + \frac{h}{2})), \quad (25)$$

$$K_{i5} = -\frac{\partial H}{\partial x_i}(t_j + \frac{3h}{4}, \lambda_i^j + \frac{1}{8}(K_1 + K_2 + 4K_3), x_i^j + \frac{1}{8}(K_1 + K_2 + 4K_3), u_s(t_j + \frac{3h}{4})), \quad (26)$$

$$K_{i6} = -\frac{\partial H}{\partial x_i}(t_j + \frac{3h}{4}, \lambda_i^j + \frac{1}{8}(3K_2 + 2K_3 - K_4 + 2K_5), x_i^j + \frac{1}{8}(3K_2 + 2K_3 - K_4 + 2K_5), u_s(t_j + 3h4)), \quad (27)$$

$$K_{i7} = -\frac{\partial H}{\partial x_i}(t_j + h, \lambda_i^j + \frac{1}{7}(K_1 - 2K_2 + 4K_3 + 4K_6), x_i^j + \frac{1}{7}(K_1 - 2K_2 + 4K_3 + 4K_6), u_s(t_j + h)), \quad (28)$$

$$\lambda_i^{j-1} = \lambda_i^j - \frac{h}{90}(7K_1 + 32K_3 + 12K_4 + 16K_5 + 16K_6 + 7K_7). \quad (29)$$

1.4: RK6 Forward-Backward Algorithm for Optimal Control Problem

Step 1: Initialization Input

$x_i(t_0) = x_i^0, \ \ \lambda_i(N) = 0 \ \forall i = 1, 2, \cdots, n, \ T, \ t_0, \ u_r(t_0) = u_r^0, \ \forall r = 1, 2, \cdots, m$

Step 2: Forward Sweep for state variables

Compute while $k = 0,1,2,...,N$ do x_i^{i+1} from equations (10) to (17) respectively and sequentially.

Step 3: Backward Sweep for adjoint variables

Set $j = N + 2 - i$ and compute $\lambda^{j}{}_i^{-1}$ from equations (22) to (29) respectively *Step 4: Control Characterization*

Compute control within bounds $u_r^* = \min\{\max\{u_{min}, u_r, \}, u_{max}\}$ for $r = 1, \cdots, m$ from equation (18)

Step 5: Termination criteria

If termination conditions are met go to step 6 otherwise step 7

Step 6: Output $x^k{}_i, \lambda^j{}_i, u^*{}_i (\forall i,j)$ and end function *Step 7: Return* Repeat step 2

2: Numerical simulations: Implementation and Results

Example 1: Considering the optimal control problem below

$$\text{Min } J[u] \quad = \quad \min \int_0^1 u(t)2 \, dt,$$

$$x'(t) \quad = \quad x(t) + u(t), \quad (30)$$

$$x(0) = 1, x(1) \text{ free.}$$

The Hamiltonian function H is defined as $H = u(t)^2 + \lambda(t)\cdot(x(t)+u(t))$ where $\lambda(t)$ is the adjoint variable (or costate). Using the optimality adjoint and transversality conditions yields the analytical (exact) optimal solution below:

$$x^*(t) = e^t, \qquad u^*(t) = 0. \tag{31}$$

The optimal control obtained using the optimality condition, $\frac{\partial H}{\partial u} = 0$, is given by

$$\begin{aligned} u^*(t) &= -\frac{\lambda(t)}{2}, \\ &= \min\left(u_{\max}, \max\left(u_{min}, -\frac{\lambda(t)}{2}\right)\right) \end{aligned} \tag{32}$$

ascertained to be minimum since $\frac{\partial^2 H}{\partial u^2} = 2 > 0.$

The derived costate equation using the adjoint conditions, $\lambda'(t) = -\frac{\partial H}{\partial I(t)}$, given by:

$$\lambda'(t) = -\lambda(t), \quad \lambda(T) = 0 \tag{33}$$

Applying the forward Euler, RK4 and the proposed RK6 forward -backward sweep methods (i.e RK4FBSM and proposed RK6FBSM respectively) yields the results below.

Table1: Result of State variable for example 1

S/N	**Exact**	**Euler**		**RK4FBSM**		**Proposed RK6FBSM**	
	x_A	x_E	$\lvert x_A - x_E\rvert$	$xK4$	$\lvert xA - xK4\rvert$	$xK6$	$\lvert xA - xK6\rvert$
1	1.1051709181	1.1111111111	$5.9401930000 \times 10^{-3}$	1.1051708333	8.47000×10^{-8}	1.1051709181	0.00000×10^{0}
2	1.2214027582	1.2345679012	$1.3165143100 \times 10^{-2}$	1.2214025709	1.87300×10^{-7}	1.2214027582	0.00000×10^{0}
3	1.3498588076	1.3717421125	$2.1883304900 \times 10^{-2}$	1.3498584971	3.10500×10^{-7}	1.3498588076	0.00000×10^{0}
4	1.4918246976	1.5241579028	$3.2333205100 \times 10^{-2}$	1.4918242401	4.57600×10^{-7}	1.4918246977	0.00000×10^{0}
5	1.6487212707	1.6935087808	$4.4787510100 \times 10^{-2}$	1.6487206386	6.32100×10^{-7}	1.6487212707	0.00000×10^{0}
6	1.8221188004	1.8816764232	$5.9557622800 \times 10^{-2}$	1.8221179621	8.38300×10^{-7}	1.8221188004	0.00000×10^{0}
7	2.0137527075	2.0907515813	$7.6998873800 \times 10^{-2}$	2.0137516266	1.08090×10^{-6}	2.0137527075	0.00000×10^{0}
8	2.2255409285	2.3230573125	$9.7516384100 \times 10^{-2}$	2.2255395633	1.36520×10^{-6}	2.2255409285	0.00000×10^{0}
9	2.4596031112	2.5811747917	$1.2157168060 \times 10^{-1}$	2.4596014138	1.69740×10^{-6}	2.4596031112	0.00000×10^{0}
10	2.7182818285	2.8679719908	$1.4969016230 \times 10^{-1}$	2.7182797441	2.08430×10^{-6}	2.7182818285	0.00000×10^{0}

Table 1: $\lvert x_A - x_E\rvert$, $\lvert x_A - x_{K4}\rvert$and$\lvert x_A - x_{K6}\rvert$ ≡ errors of Euler RK4 & RK6 respectively

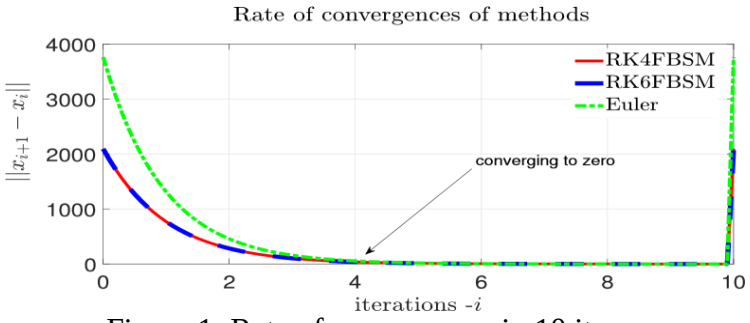

Figure 1: Rate of convergence in 10 iters.

Example 2: Considering the SIS Model with Treatment [9]

$$\min C[u] = \int_0^T \omega_1 I(t) + u^2(t)) \, dt,$$
$$s.t : \dot{I}(t) = \beta \ (N - I(t))I(t) - (\mu + \gamma)I(t) - u(t)I(t) \quad (34)$$
(35)

$$I(0) = I_0, I(T) free. \quad (36)$$

The Hamiltonian is given by:

$H(I(t),u(t),\lambda(t)) = \omega_1 I(t) + u^2(t) + \lambda(t)(\beta(N - I(t))I(t) - (\mu + \gamma)I(t) - u(t)I(t)$(37) The optimal control obtained using the optimality condition, $\frac{\partial H}{\partial u} = 0$, is given by

$$u^*(t) = \frac{\lambda(t)I(t)}{2},$$
$$= \min\left(u_{\max}, \max\left(u_{min}, \frac{\lambda(t)I(t)}{2}\right)\right). \quad (38)$$

ascertained to be minimum since $\frac{\partial^2 H}{\partial u^2} = 2 > 0.$

The derived co-state equation using the adjoint conditions, $\lambda'(t) = -\frac{\partial H}{\partial I(t)}$, given by:

$\lambda'(t) = -\omega_1 - \lambda(t)\beta(N - I(t)) - \beta I(t) - (\mu + \gamma) - u(t)$, $\lambda(T) = 0$ (39)

Applying the forward Euler, RK4 and the proposed RK6 forward -backward sweep methods (i.e RK4FBSM and proposed RK6FBSM respectively) also yields the results in Table 2 below using the following parameters: $\beta = 0.05$, $\mu = 0.01$, $\gamma = 0.5$, $N = 100$, $\omega_1 = 1$ and $T = 1$.

Table 2: Result of State and Control variables for example 2

S/N	Euler		convergence		Proposed RK6FBSM	
	x_E	u_E	$xK4$	$uK4$	$xK6$	$uK6$
1	10.0000000000	5.2355651638	10.0000000000	4.5926947060	10.0000000000	4.6363573386
2	8.7650656568	4.6326137300	9.5613737942	4.3167361686	9.5464589222	4.3768363778
3	8.2556597311	4.1600567381	9.4089685710	4.0418362859	9.3440040276	4.1061078144
4	8.1851105244	3.7431700492	9.5201882548	3.7594888052	9.3763319652	3.8164326820
5	8.4592147545	3.3460084781	9.9038244602	3.4602903181	9.6519009702	3.4992076079
6	9.0673116818	2.9449889133	10.6018768364	3.1325900058	10.2060033528	3.1440596831
7	10.0557266500	2.5197980734	11.7007294372	2.7604692418	11.1093962855	2.7374992954
8	11.5303031948	2.0484433716	13.3574883436	2.3201655255	12.4871637697	2.2605946027

9	13.6800933636	1.5026879752	15.8577984930	1.7728678617	14.5571182701	1.6844954512
10	16.8306930352	0.8415968385	19.7510850824	1.0482398348	17.7109254612	0.9609642283
11	21.5547425985	0.0000000000	26.2132226347	0.0000000000	22.7016008493	0.0000000000

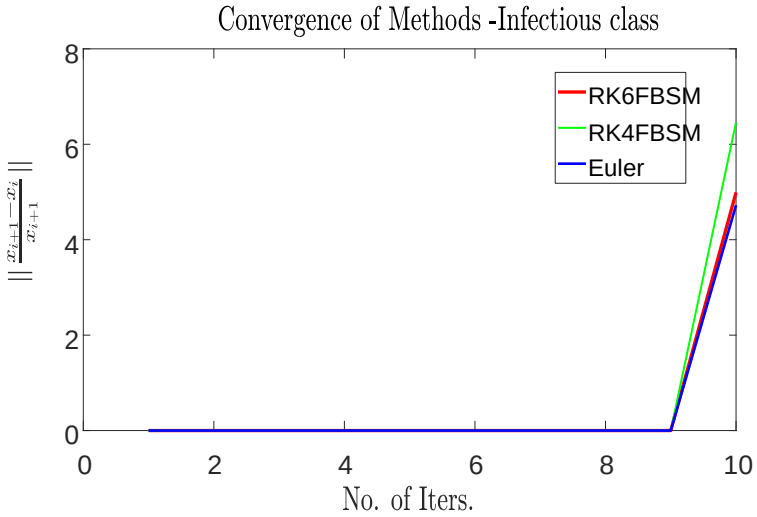

Figure 2: Rate of convergence in 10 iterations.

Example 3: We considered the model on optimal control and comprehensive cost effectiveness analysis for COVID-19 [2]

$$J(u_1,u_2,u_3,u_4) := \min \int_0^T \left[A_1E + A_2I + A_3A + A_4B + \frac{1}{2}\sum_{i=1}^{4} D_i u_i^2(t) \right] dt \tag{40}$$

Subject to the non-autonomous system below

$$\begin{cases} \frac{dS}{dt} &= \Lambda - (1-u_1(t))\left(\frac{\beta_1 E + \beta_2 I + \beta_3 A}{N}\right) S - (1-u_1(t)-u_2(t))\frac{\beta_4 B}{N} S - dS, \\ \frac{dE}{dt} &= (1-u_1(t))\left(\frac{\beta_1 E + \beta_2 I + \beta_3 A}{N}\right) S + (1-u_1(t)-u_2(t))\frac{\beta_4 B}{N} S - (\delta+d)E, \\ \frac{dI}{dt} &= (1-\tau)\delta E - (d+d_1+\gamma_1)I, \\ \frac{dA}{dt} &= \tau\delta E - (d+\gamma_2)A, \\ \frac{dR}{dt} &= \gamma_1 I + \gamma_2 A - dR, \\ \frac{dB}{dt} &= (1-u_3(t))(\psi_1 E + \psi_2 I + \psi_3 A) - (u_4(t)+\phi)B, \end{cases} \tag{41}$$

where $A_i > 0 (i = 1,2,3,4)$. The derived adjoint equations were

$$\begin{cases} \frac{d\lambda_1}{dt} = (\lambda_1-\lambda_2)((1-u_1)(\frac{\beta_1 E^* + \beta_2 I^* + \beta_3 A^*}{N^2})(E^*+I^*+A^*+R^*)) + \\ (\lambda_1-\lambda_2)(1-u_1-u_2)\frac{\beta_4 B^*}{N^2}(E^*+I^*+A^*+R^*) + \lambda_1 d, \\ \frac{d\lambda_2}{dt} = -A_1 + (\lambda_1-\lambda_2)(1-u_1)S^*(\frac{S^*+I^*+A^*+R^*}{N^2}\beta_1 - \beta_2 I^* + \beta_3 A^*) + \\ (\lambda_2-\lambda_1)(1-u_1-u_2)\frac{\beta_4 B^* S^*}{N^2} + (\delta+d)\lambda_2 - \lambda_2(1-\tau)\delta\lambda_3 - \tau\delta\lambda_4 - (1-u_3)\psi_1\lambda_6 \\ \frac{d\lambda_3}{dt} = -A_2 + (\lambda_1-\lambda_2)(1-u_1)S^*(\frac{(S^*+E^*+A^*+R^*\beta_2 - \beta_1 E^* + \beta_3 A^*)}{N^2}) + \\ (\lambda_2-\lambda_1)(1-u_1-u_2)\frac{\beta_4 B^* S^*}{N^2} + (\delta+d_1+\gamma_1)\lambda_3 - \gamma_1\lambda_5 - (1-u_3)\psi_2\lambda_6, \\ \frac{d\lambda_4}{dt} = -A_3 + (\lambda_1-\lambda_2)(1-u_1)S^*(\frac{(S^*+E^*+I^*+R^*\beta_3 - \beta_1 E^* + \beta_2 I^*)}{N^2}) + \\ (\lambda_2-\lambda_1)(1-u_1-u_2)\frac{\beta_4 B^* S^*}{N^2} + (d_1+\gamma_2)\lambda_4 - \gamma_2\lambda_5 - (1-u_3)\psi_3\lambda_6, \\ \frac{d\lambda_5}{dt} = (\lambda_2-\lambda_1)(1-u_1)(\frac{\beta_1 E^* + \beta_2 I^* + \beta_3 A^*)S^*}{N^2}) + \\ (\lambda_2-\lambda_1)(1-u_1-u_2)\frac{\beta_4 S^*}{N^2} + \lambda_5 d, \\ \frac{d\lambda_6}{dt} = -A_4 + (\lambda_1-\lambda_2)(1-u_1-u_2)\frac{\beta_4 S^*}{N} + (u_4+\phi)\lambda_6 d, \end{cases} \tag{42}$$

while the optimal control characterizations were;

$$
\begin{aligned}
u_1^*(t) &= \min\left\{\max\left\{0, \frac{(\lambda_2-\lambda_1)(\beta_1 E^* + \beta_2 I^* + \beta_3 A^* + \beta_4 B^*)S}{D_1 N}\right\}, u_{1\max}\right\}\\
u_2^*(t) &= \min\left\{\max\left\{0, \frac{(\lambda_2-\lambda_1)\beta_4 B^* S^*}{D_2 N}\right\}, u_{2\max}\right\},\\
u_3^*(t) &= \min\left\{\max\left\{0, \frac{\lambda_6(\psi_1 E^* + \psi_2 I^* + \psi_3 A^*)}{D_3}\right\}, u_{3\max}\right\},\\
u_4^*(t) &= \min\left\{\max\left\{0, \frac{\phi B^* \lambda_6}{D_4}\right\}, u_{4\max}\right\}.
\end{aligned}
\tag{43}
$$

Simulating with the following parameters $\beta_1 = 0.1233$;$\beta_2 = 0.0542$;$\beta_3 = 0.0020$;$\beta_4 = 0.1101$;$\delta = 0.1980$;$\tau = 0.3085$;$d = 1/(74.87 * 365)$;$d_1 = 0.0104$;$\gamma_1 = 0.3680$;$\gamma_2 = 0$;$\psi_1 = 0.2574$;$\psi_2 = 0.2798$;$\psi_3 = 0.1584$;$\phi = 0.3820$ yields the results below.

Table 3: Convergence analysis of State variable ($E(t)$) for example 3

S/N	**Euler**		**RK4FBSM**		**Proposed RK6FBSM**	
	E_E	$\|\frac{E_{i+1}-E_i}{E_{i+1}}\|$	$EK4$	$\|\frac{E_{i+1}-E_i}{E_{i+1}}\|$	$EK6$	$\|\frac{E_{i+1}-E_i}{E_{i+1}}\|$
1	1.5000000000	-	1.5000000000		1.5000000000	
11	1.4586854415	2.7646377×10^{-3}	1.4582818367	2.7890189×10^{-3}	1.4581829510	2.7953366×10^{-3}
21	1.4194850125	2.6987961×10^{-3}	1.4187988721	2.7167244×10^{-3}	1.4186243717	2.7216273×10^{-3}
31	1.3821955578	2.6394372×10^{-3}	1.3813219909	2.6520393×10^{-3}	1.3810945185	2.6556630×10^{-3}
41	1.3466385402	2.5859736×10^{-3}	1.3456514066	2.5942269×10^{-3}	1.3453892655	2.5968128×10^{-3}
51	1.3126570130	2.5378496×10^{-3}	1.3116129021	2.5425930×10^{-3}	1.3113294894	2.5443931×10^{-3}
61	1.2801128162	2.4946384×10^{-3}	1.2790541427	2.4967666×10^{-3}	1.2787595421	2.4977039×10^{-3}
71	1.2488168407	2.4685349×10^{-3}	1.2477535795	2.4713852×10^{-3}	1.2474913995	2.4675198×10^{-3}
81	1.2184644912	2.4616005×10^{-3}	1.2173844274	2.4656931×10^{-3}	1.2171894367	2.4600497×10^{-3}
91	1.1893046217	2.3341404×10^{-3}	1.1885613052	2.2797627×10^{-3}	1.1883097475	2.2930852×10^{-3}
101	1.1685184378	1.2045593×10^{-3}	1.1684734094	1.2114794×10^{-3}	1.1676305020	1.2714446×10^{-3}

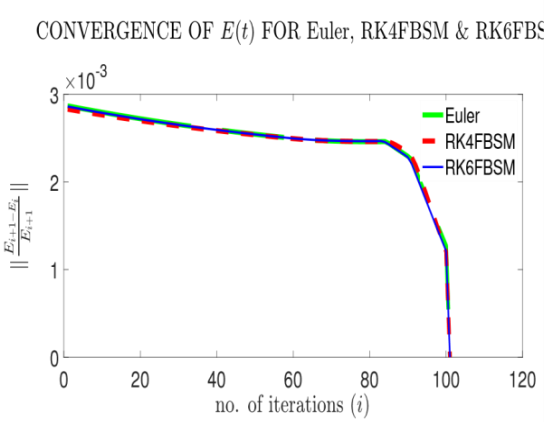

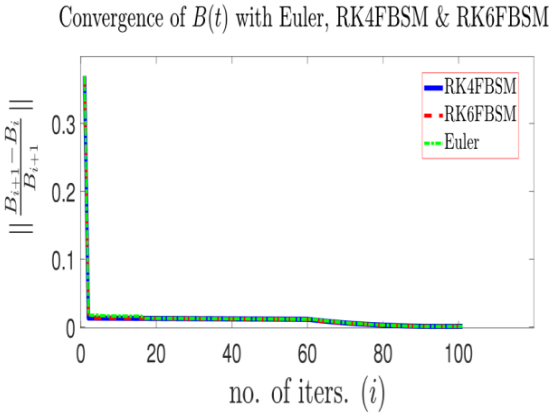

Fig. 3: Convergence of *E*(*t*) in 101 iterations. Fig 4: Convergence of *B*(*t*) in 101 iterations.

DISCUSSION OF RESULTS

In example 1, the rate of convergence of the 3 methods: Euler, RK4 and Rk6 were compared on the state variable as demonstrated on table 1. It was discovered that the rate of convergence of the RK6 compares favorably with RK4 with higher level of accuracy after 10 iterations. In similar manner, Table 2 and 3 were used to compare the Iterates for the Euler, RK4 and RK6 forward-backward sweep methods on the state variables of examples 2 and 3 respectively. Figures 2, 3 and 4 were used to illustrate the rate of convergences which shows that the RK6FBSM performs excellently well although the computational efforts is more in terms of rigors of coding and process time.

CONCLUSION

The adaptation of the 6th order Runge-Kutta forward-backward sweep algorithm for solving generalized optimal control problems with bounded control arrives at an accurate result at a faster rate of convergence compared to the Runge-Kutta of order four (RK4), due to its stability and higher numerical order of convergence. This adaptation is essential for handling mathematical models with large number of non-linear dynamical equations. Therefore, the sixth order Runge-Kutta forward-backward sweep algorithm seeks to provide a more effective and efficient method due to its speed, accuracy, higher rate of convergence, suitability and versatility for real-time or practical applications such as the Epidemiological and general Biomedical models (see MATLAB code in Appendix).

REFERENCES

1. Adamu, S. (2023). Numerical solution of optimal control problems using block method. Electronic Journal of Mathematical Analysis and Applications, 11(2), 8. ISSN: 2090729X (online). Retrieved from http://ejmaa.journals.ekb.eg

2. Asamoah, J. K., Okyere, E., Abidemi A., Moore, S. E., Sun, G.,, Jin,, Z., Acheampong, E. and GordonOptimal, J. F. (2022), Control and comprehensive costeffectiveness analysis for COVID-19

3. Banu, M. S., Raju, I. and Mondal, S. (2021). A comparative study on classical fourth order and Butcher sixth order Runge-Kutta methods with initial and boundary value problems. International Journal of Material and Mathematical Sciences, 2(1), 8-21. https://doi.org/10.34104/ijmms.021.08021

4. Berkovitz, L. D. (1962). On control problems with bounded state variables. Journal of Mathematical Analysis and Applications, 5, 488-498. https://core.ac.uk/display/82704868

5. Guzman D´ıaz, D., Gomez-Aleixandre, J. and Coto, J. (2015). Direct backward/forward sweep algorithm for solving load power flows in AC droopregulated microgrids. IEEE Transactions on Power Systems, 30(6), 3151-3160. https://www.researchgate.net/publication/282530636

6. Kirk, D. E. (2004). Optimal control theory: An introduction . Dover Publications . 184-240. Retrieved from https://dokumen.tips/documents/optimal-control-theoryan-introduction.html?page=2

7. La Torre, D., Kunze, H., Ruiz-Galan, M., Malik, T. and Marsiglio, S. (2015). Optimal Control: Theory and Application to Science, Engineering, and Social Sciences. Abstract and Applied Analysis, 890527. https://doi.org/10.1155/2015/890527

8. Lenhart, S., & Workman, J. T. (2007). Optimal control applied to biological models (Chapman & Hall/CRC Mathematical and Computational Biology Series). Chapman and Hall/CRC. Retrieved from https://dokumen.pub/download/optimalcontrol-applied-to-biological-models-9781322628394-1322628394-978-1-4200-1141-8-

9. 1420011413 .html

10. Martcheva, M. (2015). An introduction to mathematical epidemiology (Texts in Applied Mathematics 61). Springer Science+Business Media New York, p. 237. https://doi.org/10.1007/978-1-4899-7612-3

11. Pontryagin,L. S., Boltyanskii, V. G., Gamkrelize, R. V. and Mishchenko, E. F. (1962). The Mathematical Theory of Optimal Processes. Wiley, New York.

12. Rose, G. R. (2015). Numerical Methods for Solving Optimal Control Problems. Master's Thesis, University of Tennessee. Retrieved from https://trace.tennessee.edu/utk$_g$radthes/3401.